Electron capture into large-*l* Rydberg states of multiply charged ions escaping from solid surfaces

N. N. Nedeljković, Lj. D. Nedeljković, and M. A. Mirković*
Faculty of Physics, University of Belgrade, P.O. Box 368, Belgrade, Yugoslavia
(Received 15 May 2002; published 25 July 2003)

We have investigated the electron capture into large-*l* Rydberg states of multiply charged ionic projectiles (e.g., the core charges $Z=6$, 7, and 8) escaping solid surfaces with intermediate velocities ($v\approx 1$ a.u.) in the normal emergence geometry. A model of the nonresonant electron capture from the solid conduction band into the moving large angular-momentum Rydberg states of the ions is developed through a generalization of our results obtained previously for the low-*l* cases ($l=0$, 1, and 2). The model is based on the two-wave-function dynamics of the Demkov-Ostrovskii type. The electron exchange process is described by a mixed flux through a moving plane (''Firsov plane''), placed between the solid surface and the ionic projectile. Due to low eccentricities of the large-*l* Rydberg systems, the mixed flux must be evaluated through the whole Firsov plane. It is for this purpose that a suitable asymptotic method is developed. For intermediate ionic velocities and for all relevant values of the principal quantum number $n\approx Z$, the population probability P_{nl} is obtained as a nonlinear *l* distribution. The theoretical predictions concerning the ions S VI, Cl VII, and Ar VIII are compared with the available results of the beam-foil experiments.

DOI: 10.1103/PhysRevA.68.012721 PACS number(s): 34.50.Fa, 34.50.Dy, 79.20.Rf

I. INTRODUCTION

Interactions of multiply charged ions or Rydberg atoms with solid surfaces have attracted considerable attention over the past decade. A number of theoretical studies that have appeared in the literature deal with the problem of electron capture and recapture at low velocities ($v\ll 1$ a.u.). The classical over barrier model [1,2] and its extended dynamic version [3,4] reflect global physical aspects of the problem. The quantum descriptions of the resonant charge exchange have been focused on calculating the transition matrix elements and transition rates [5] as well as basic matrix elements [6] within the framework of the perturbative models. The coupled angular mode method [7] and the complex scaling method [8] have been used in the nonperurbative calculations of the energy shifts and widths. Also, the mixing of the *l* states and the most active members of the *n* manifolds can be recognized by the last two methods.

On the other hand, the analysis of the Rydberg state population of multiply charged ions traversing thin foils at high velocities ($v\gg 1$ a.u.) has indicated that the bulk effects are relevant under these experimental conditions. The high-*l* Rydberg states, observed as a result of the beam-foil interaction, have been treated within the framework of classical transport theory [9].

Recently, a theoretical study [10,11] of the one-electron capture into the Rydberg states of multiply charged ions at intermediate velocities ($v\approx 1$ a.u.) has been carried out. This analysis has been motivated by a series of beam-foil experiments [12–14] with the ionic projectiles characterized by the core charges $Z=6$, 7, and 8, not yet studied by the above cited models. The absence of any explanation of the experiments [12–14] by the methods [1–8] indicated to us that the resonant mechanism could not be sufficient for a complete description of the charge exchange process in the intermediate velocity region. In particular, we realized that the intermediate stages of the ion-surface interaction, under the mentioned beam-foil conditions, require more details in quantum dynamics based on the nonresonant electron-capture mechanism. Moreover, we observed that the experimentally available *l* distributions of the Rydberg states at $v\approx 1$ a.u. are qualitatively different from the theoretical results for fast ions ($v\approx 10$ a.u.) obtained within classical transport theory [9].

Taking into account the above facts, we analyzed the experimental data [12–14] as a surface effect, considering the electron-capture process along the outgoing part of the ionic trajectory. Our model [10,11,15] is based on a generalization of the Demkov-Ostrovskii methodology [16], used previously in the theory of atomic collisions. The electron-capture probability is expressed [15] in terms of a mixed flux $I(t)$ through a moving ''Firsov'' plane S_F, placed between the ionic projectile and the backside of the foil. The position of the Firsov plane is not arbitrary, but is chosen such that it separates the space where the foil potential is strong, from the space where the atomic potential is strong, i.e., qualitatively, the plane is placed in the ''interaction-free'' region between the foil and the atom.

To calculate the flux $I(t)$ we need two wave functions $\Psi_1(\vec{r},t)$ and $\Psi_2(\vec{r},t)$ of an active electron. While the first function evolves from an initial electron state at $t=t_{in}$, the second function represents a state that evolves towards a fixed final electron state at $t=t_{fin}$. In the proposed two-wave-function dynamics, for the evaluation of physically relevant quantities it is sufficient to know the states Ψ_1 and Ψ_2 exclusively on the S_F plane. Let us note that a ''volume calculation'' for a transition amplitude can also be converted to a ''surface calculation'' within the framework of the Bardeen transfer Hamiltonian method [17], but considering the quasistationary transition problem.

The model [10,11] of electron captures from the foil valence band into moving bound states (with $n\approx Z$), however,

*Electronic address: hekata@ff.bg.ac.yu

has been developed by restricting to the case of low-l Rydberg states (e.g., $l=0$, 1, and 2). Namely, in the low-l case the ionic Rydberg states have large eccentricities so that only a narrow cylindrical region around the ionic trajectory is relevant for the electron-capture process. Accordingly, it has been possible [10,11] to calculate the mixed electron flux $I(t)$ through the S_F plane by restricting our analysis exclusively to the central part of that plane. The population probability P_{nl} at $t=t_{fin}\to\infty$, determined completely by the mixed flux, has been calculated and compared with experiments. All available low-l experimental facts concerning the ions S VI, Cl VII, and Ar VIII have been reproduced by the model.

Under the mentioned experimental conditions [12–14], the large-l Rydberg state population ($l\geqslant 3$) represents a more complicated problem in comparison to the low-l case. In order to simplify the analysis of the experimental data, we shall distinguish two physically different cases of the large-l distributions corresponding to the Rydberg states with fixed values of the quantum number n. In the first case, the experimental curves have an upper limit at $l_{max}=n-1$ for all tested values of the ionic core charges and velocities. This kind of large-l distributions is characteristic for lower-n values (roughly, $5<n<7$ or 8) of the ionic projectiles S VI, Cl VII, and Ar VIII. We realized that the electron-capture mechanism is dominant under these conditions. In the second case, however, the large-l distributions have the upper limits $l_{thr}<n-1$, indicating that an additional, reionization-type process [11,18] is active inside the ion-surface system. This kind of large-l distributions prevails in the case of higher-n values of the Rydberg states of the ions S VI and Cl VII, and especially for the Ar VIII ion.

In this paper, we present a generalization of the low-l model [10,11] to the large-l Rydberg systems. Due to the complexities of interplay between the electron-capture and reionization processes (requiring a separate analysis), we shall restrict ourselves to the lower-n cases where the electron-capture process is dominant. Heuristically, the following two facts determine the electron-capture dynamics under the mentioned conditions. Namely, the large-l Rydberg states are characterized by very small eccentricities and we can expect that the space region of the electron transitions extends far from the ionic trajectory. Beside this, the electron capture into a moving Rydberg state occurs at large ion-surface distances $R\gg 1$, which indicates that an asymptotic methodology can be used in the study of the process. Accordingly, in contrast to the low-l case, we need the mixed flux through the whole S_F plane. This means that sufficiently accurate asymptotic expressions for wave functions $\Psi_1(\vec{r},t)$ and $\Psi_2(\vec{r},t)$, valid on the entire Firsov plane, must be found.

The evaluation of functions $\Psi_1(\vec{r},t)$ and $\Psi_2(\vec{r},t)$ on the S_F plane is performed by means of a suitable asymptotic method. These functions are obtained by an analytical continuation from the regions where they are mainly localized (the solid region and the ionic core vicinity, respectively) to the whole Firsov plane. A similar procedure has been used previously in the case of proton neutralization at solid surfaces [15]. Using the obtained functions we calculate the mixed flux for large-l Rydberg states, from which the experimentally verifiable population probability can be obtained.

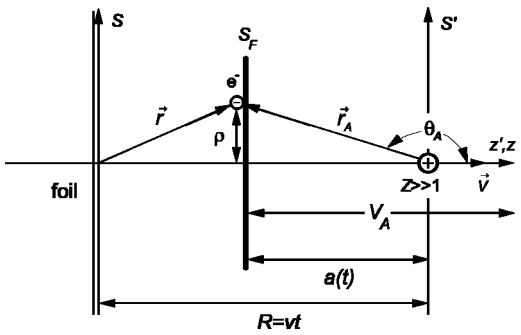

FIG. 1. Geometry of the process.

This paper is organized as follows. In Sec. II, we formulate the electron-capture problem, exposing the large-l dynamics and the asymptotic procedure. An explicit model of the large-l Rydberg state population is developed and compared with experiments in Sec. III. Some concluding remarks will be given in Sec. IV.

Atomic units ($e^2=\hbar=m_e=1$) will be used throughout the paper unless indicated otherwise.

II. FORMULATION OF THE PROBLEM

A. Large-l quantum dynamics

The two-state model of electron captures into Rydberg states of multiply charged ions escaping solid surfaces has been explicated in more detail in our previous papers [10,11]. Here we expose the facts relevant to the population of the large-l Rydberg states.

In Fig. 1, we present the process in a normal emergence geometry, taking that the pointlike projectile $Z\gg 1$ moves with intermediate velocities according to the classical law $R=vt$. The instant position of the S_F plane with respect to the ion is denoted by $a(t)$. We indicate the ionic region by V_A. For the large-l Rydberg states, all parts of the S_F plane are relevant, including those with large values of the radial coordinate ρ.

The active electron is described simultaneously by the states $|\Psi_1(t)\rangle=\hat{U}(t_{in},t)|\Psi_1(t_{in})\rangle$ and $|\Psi_2(t)\rangle=\hat{U}(t_{fin},t)|\Psi_2(t_{fin})\rangle$. The evolution operators $\hat{U}(t_{in},t)$ and $\hat{U}(t_{fin},t)$ are determined by the one-electron Hamiltonians $\hat{H}_1(t)$ and $\hat{H}_2(t)$:

$$\hat{H}_1(t)=-\frac{1}{2}\nabla^2+U_M+(U_A+U_{AM}), \tag{2.1a}$$

$$\hat{H}_2(t)=-\frac{1}{2}\nabla^2+U_A+[U_M\Theta(z)+U_{AM}]. \tag{2.1b}$$

The regions inside and outside the solid are defined by the Heaviside function $\Theta(z)$. We denoted the Coulomb potential of the electron-ionic core interaction by U_A, whereas $U_M=-U_0\Theta(-z)-(4z)^{-1}\Theta(z)$ is the electron-solid interac-

tion potential, and U_{AM} is the interaction potential of the active electron with the ionic core image.

The intermediate stages of the electron-capture process can be described [10,11,15,16] by the probability that the single active electron, whose behavior is determined simultaneously by the state vectors $|\Psi_1(t)\rangle$ and $|\Psi_2(t)\rangle$, is in the atomic region V_A. The related probability amplitude is given by

$$A(t)=\langle\Psi_2(t)|\hat{P}_A|\Psi_1(t)\rangle, \tag{2.2a}$$

where the projection operator $\hat{P}_A$ (in the coordinate representation) is specified by the Heaviside function $\Theta(z-R+a)$. For a large-l Rydberg state, the amplitude $A(t)$ can be expressed as

$$A(t)=\int_{t_g}^{t} I(t)dt, \tag{2.2b}$$

where the mixed flux $I(t)$ is given by the following surface integral over the Firsov plane:

$$I=\frac{i}{2}\int_{S_F}\left[\frac{\vec{\nabla}\Psi_1}{\Psi_1}-\frac{\vec{\nabla}\Psi_2^*}{\Psi_2^*}-2iv\left(1-\frac{da}{dR}\right)\vec{e}_z\right]\Psi_2^*\Psi_1\cdot d\vec{S}, \tag{2.3}$$

where $d\vec{S}=dS\vec{e}_z$ and $\vec{e}_z$ is the unit vector of the z axis. In Eq. (2.2b), we took into account the fact that the population practically begins at $t=t_g\neq 0$. The parameter t_g will be determined by means of energetic arguments (Sec. III C). Note that the quantity $I=I(t,a(t))$ represents a functional of the position $a(t)$ of the S_F plane.

We consider the active electron which is initially in a state defined by the set $\mu_{M,in}=(\gamma_{in},n_{1M,in},m_{M,in})$ of the parabolic quantum numbers, where γ_{in} is the continuous energy parameter, i.e., the initial electron energy is given by $E^{(1)}_{M,in}=-\gamma^2_{in}/2$. The ionic Rydberg state, detected at $t=t_{fin}\to\infty$, is described by the index set $\nu_{A,fin}=(n,l,m)$ of spherical quantum numbers. The final eigenenergy is given by $E^{(2)}_{A,fin}=-\gamma^2_{A0}/2$, where $\gamma_{A0}=Z/n$ is the corresponding discrete energy parameter. Therefore, we define [10,11,15,16] the following neutralization probability $T^N(t)$ per unit γ_{in}:

$$T^N(t)=T^{N,\mu_{M,in}}_{\nu_{A,fin}}(t)=|A(t)|^2. \tag{2.4a}$$

The neutralization rate $\Gamma^N(t)$ per unit γ_{in} is given by

$$\Gamma^N(t)=\Gamma^{N,\mu_{M,in}}_{\nu_{A,fin}}(t)=dT^{N,\mu_{M,in}}_{\nu_{A,fin}}(t)/dt. \tag{2.4b}$$

Note that the quantities given by Eqs. (2.4a) and (2.4b) depend, for all $t\in[t_{in},t_{fin}]$, not only on the initial condition but also on the fixed final condition at the time $t_{fin}\to\infty$.

The experimentally verifiable population probability P_{nl} of the Rydberg state $\nu_{A,fin}$ from all valence-band states of the solid is determined by

$$P_{nl}=\int\sum_{\mu_{M_{in}}}\sum_{m}T^{N,\mu_{M,in}}_{\nu_{A,fin}}(t)d\gamma_{in},\quad t\to\infty. \tag{2.4c}$$

Let us note that for $t=t_{fin}\to\infty$ we have $\hat{P}_A|\Psi_2(t)\rangle=|\Psi_2(t)\rangle$, which means that the amplitude $A(t)$ tends towards the transition amplitude $A=\langle\Psi_2(t_{fin})|\Psi_1(t_{fin})\rangle$ of the process. Therefore, for $t=t_{fin}$, the probability P_{nl} obtains the standard quantum-mechanical form.

From the scheme presented, we recognize a technically significant role of the Firsov plane within the framework of the two-state model proposed. Namely, the mixed flux $I(t)$, Eq. (2.3), as well as $\Gamma^N(t)$ and P_{nl} are completely determined by the values of wave functions Ψ_1 and Ψ_2 on that plane. This fact considerably simplifies the subsequent calculations, because it is not necessary to have the functions in the entire space. The instant position of the Firsov plane is determined [10] by the variational requirement $\delta P_{nl}/\delta a=0$, with the boundary conditions $\delta a(t_{in})=0$ and $\delta a(t_{fin})=0$. Explicit calculations concerning the kinematics of the S_F plane are presented in Sec. IV A of Ref. [10]. For the experimental situation discussed in this paper (large l, but lower-n values of the Rydberg states of the ions S VI, Cl VII, and Ar VIII, see Introduction), the instant position $a=a(t)$ of the S_F plane is determined with sufficient accuracy by Eq. (4.20) of Ref. [10].

B. The asymptotic procedure

The electron-capture model exposed in Sec. II A is formulated exclusively within the framework of quantum dynamics on the S_F plane. For large ion-surface distances R, where the Rydberg state populations are dominant, the Firsov plane is located far from both the solid surface and the ionic core. For this reason, the functions $\Psi_1(\vec{r},t)$ and $\Psi_2(\vec{r},t)$ figuring in the mixed flux $I(t)$, Eq. (2.3), can be represented in the vicinity of the S_F plane by corresponding asymptotic forms ($R\gg 1$, $r\gg 1$, and $r_A\gg 1$).

Through the process, the state $\Psi_1(\vec{r},t)$, representing an eigenstate of the Hamiltonian $\hat{H}_1(t)$ at the initial time $t=t_{in}=0$, is mainly localized inside the solid. In the vicinity of the S_F plane, and for $R\gg 1$, it can be expressed in the form

$$\Psi_1(\vec{r},t)=\exp[h_{M,\mu_M}(\vec{r},t)]\Phi^{(1)}_{MA,\mu_M}(\vec{r},R), \tag{2.5}$$

where $\Phi^{(1)}_{MA,\mu_M}(\vec{r},R)$ is the eigenfunction of the Hamiltonian $\hat{H}_1(t)$ corresponding to the eigenenergy $E^{(1)}_M(R)=-\gamma(R)^2/2$. By $\mu_M=(\gamma(R),n_{1M},m_M)$ we denoted the intermediate parabolic set satisfying the condition $\mu_M\to\mu_{M,in}$ when $t\to t_{in}$. The function $\exp[h_{M,\mu_M}(\vec{r},t)]$ represents a space-time correction factor. On the other hand, for the function $\Phi^{(1)}_{MA,\mu_M}(\vec{r},R)$ we have the following asymptotic form:

$$\Phi^{(1)}_{MA,\mu_M}=\Phi^{(1)}_{as}=\Phi^{(1)}_{M,\mu_M}(\vec{r},R)\exp[-s_M(\vec{r},R)], \tag{2.6a}$$

where $\Phi^{(1)}_{M,\mu_M}$ is the eigenfunction of the metal Hamiltonian $\hat{H}_M=-\frac{1}{2}\nabla^2+U_M$, whereas $s_M(\vec{r},R)$ represents a correction function.

An asymptotic expression of the function $\Phi^{(1)}_{M,\mu_M}$ can be obtained directly from the energy eigenvalue problem of the Hamiltonian $\hat{H}_M$ expressed in parabolic coordinates. For the parabolic quantum numbers $n_{1M}=n_{1M,in}=0$ and $m_M=m_{M,in}=0$, which give the main contribution [10,11] to the electron-capture process, we get

$$\Phi^{(1)}_{M,\mu_M}(\vec{r},R)=N_M(R)\exp(-\gamma z), \tag{2.6b}$$

where $N_M(R)$ is an unknown function of R. Note that the factor $N_M(R)$ cannot be determined by a normalization of the function $\Phi^{(1)}_{M,\mu_M}$, because the validity of Eq. (2.6b) is restricted exclusively to the vicinity of the S_F plane.

What we can do, however, is to connect expression (2.5) with the expression for $\Psi_1(\vec{r},t)$ valid inside the solid. We use the known JWKB form for the eigenfunctions $\Phi^{(1)}_{MA,\mu_M}$, obtained by the asymptotic procedure of analytic continuation from the solid region. In the region $\rho \ll 1$ of the Firsov plane, we have

$$\Phi^{(1)}_{MA,\mu_M}(\vec{r},R)=\Phi^{(1)}_{JWKB}. \tag{2.6c}$$

By equating the JWKB form (2.6c) and the asymptotic form (2.6a) of the function $\Phi^{(1)}_{MA,\mu_M}$ in the central part ($\rho \ll 1$) of the S_F plane, we obtain the function $N_M(R)$.

The correction functions s_M and h_M, figuring in the wave function $\Psi_1(\vec{r},t)$, can be calculated by using an extension of the low-l procedure [10] to the large-l case. Now, it is insufficient to consider the very vicinity of the z axis ($\rho=0$); instead, an explicit ρ dependence of the correction factors is necessary. Consequently, the exposed asymptotic procedure gives the wave function $\Psi_1(\vec{r},t)$ on the whole Firsov plane.

The function $\Psi_2(\vec{r},t)$ is mainly localized in the vicinity of the ionic core and vanishes in the solid region. Namely, the potential in the Hamiltonian $\hat{H}_2(t)$ tends to zero for $z<0$, so that the eigenfunctions of $\hat{H}_2(t)$ and, consequently, the function $\Psi_2(\vec{r},t)$, are negligible in the solid region. Therefore, in order to obtain the $\Psi_2(\vec{r},t)$ function on the Firsov plane, a connection with the solid region is not necessary. For that reason, the asymptotic procedure uses an asymptotic expression of the $\Psi_2(\vec{r},t)$ function valid in the atomic region.

The function $\Psi_2(\vec{r},t)$ in the coordinate system S and the corresponding function $\Psi'_2(\vec{r},t)$ in the moving coordinate system S' (Fig. 1) differ by the Galilean factor:

$$\Psi_2(\vec{r},t)=\exp[ivz-i(v^2/2)t]\Psi'_2(\vec{r},t), \tag{2.7a}$$

where

$$\Psi'_2(\vec{r},t)=\exp[h_{A,\nu_A}(\vec{r},t)]\Phi^{(2)}_{AM,\nu_A}(\vec{r},R). \tag{2.7b}$$

By $\Phi^{(2)}_{AM,\nu_A}$ we denoted the eigenfunction of the Hamiltonian $\hat{H}_2(t)$ corresponding to the eigenenergy $E^{(2)}_A(R)=-\gamma_A(R)^2/2$. By $\nu_A=(n_A,l_A,m_A)$ we denoted the intermediate spherical set satisfying the condition $\nu_A \to \nu_{A,fin}$ when $t \to t_{fin}$. The factor $\exp[h_{A,\nu_A}(\vec{r},t)]$ represents a space-time correction. For $t=t_{fin}\to\infty$, the state $\Psi'_2(\vec{r},t)$ turns into an eigenstate of the Hamiltonian $\hat{H}_2(t)$.

In the vicinity of the S_F plane, the function $\Phi^{(2)}_{AM,\nu_A}$ can be expressed by the following asymptotic form:

$$\Phi^{(2)}_{AM,\nu_A}=\Phi^{(2)}_{as}=\Phi^{(2)}_{A,\nu_{A,fin}}(\vec{r}_A)\exp[-s_A(\vec{r}_A,R)], \tag{2.8}$$

where $\Phi^{(2)}_{A,\nu_{A,fin}}(\vec{r}_A)$ is the eigenstate of the atomic Hamiltonian $\hat{H}_A=-\frac{1}{2}\nabla^2+U_A$. The fact that function (2.8) represents the large-l Rydberg state for $R\to\infty$ will be taken into account through an appropriate asymptotic expression for the $\Phi^{(2)}_{A,\nu_{A,fin}}(\vec{r}_A)$ function (Sec. III B).

Finally, it remains to determine the correction factors s_A and h_A in the function $\Psi'_2(\vec{r},t)$, Eq. (2.7b). For the large-l case, it will be sufficient to consider the ρ dependence of the difference h_A-s_A. In this way, we can obtain the function $\Psi_2(\vec{r},t)$, which is valid on the entire Firsov plane.

III. POPULATION OF LARGE-l RYDBERG STATES

A. The function $\Psi_1(\vec{r},t)$ on the S_F plane

In order to obtain an asymptotic form of the function $\Psi_1(\vec{r},t)$ on the whole S_F plane, we first need to calculate explicitly the eigenfunction $\Phi^{(1)}_{MA,\mu_M}(\vec{r},R)$, Eq. (2.5).

We start from the JWKB form [19] ($R\gg 1, r\gg 1$) of the function $\Phi^{(1)}_{MA,\mu_M}$ valid in the central part $\rho\approx 0$ of the S_F plane. For the quantum number $m_M=m_{M,in}=0$, giving the main contribution [10,11] to the electron transitions, we have [10]

$$\Phi^{(1)}_{JWKB}=\pi^{-1}\gamma^{1/2\gamma+1/2}e^{1/4\gamma}2^{-(2Z-1)/2\gamma+1/4\gamma-1} \times g^{-Z/\gamma+n_{1M}}R^{1/4\gamma-1/2}e^{-\gamma z}, \tag{3.1}$$

where $g=a(t)/R(t)$. Expression (3.1) has been obtained by the JWKB continuation of the function $\Phi^{(1)}_{MA,\mu_M}$ from the solid throughout the narrow cylindrical region around the z axis into the vicinity of the ionic core.

On the other hand, the eigenfunction $\Phi^{(1)}_{MA,\mu_M}$, valid for all ρ values of the S_F plane, is also determined by Eq. (2.6a). Assuming that $\nabla^2 s_M\approx 0$ and $(\vec{\nabla}s_M)^2\approx 0$, and using the asymptotic expression (2.6b), we obtain [10] the following differential equation: $\gamma\partial s_M/\partial z=U_A+U_{AM}$. The particular solution of the last equation, satisfying the condition $\lim_{R\to 0}s_M(\vec{r},R)=0$, is given by

$$s_M=\frac{Z}{\gamma}\ln\left(\frac{\sqrt{\rho^2+(R-z)^2}+R-z}{\sqrt{\rho^2+R^2}+R}\right) +\frac{Z}{\gamma}\ln\left(\frac{\sqrt{\rho^2+(R+z)^2}+R+z}{\sqrt{\rho^2+R^2}+R}\right), \tag{3.2}$$

where $a/R \to 1$ for $R \to 0$. Note that we have $z = R - a$ on the Firsov plane.

In the vicinity of the Firsov plane, the asymptotic form $\Phi^{(1)}_{as}$ of the function $\Phi^{(1)}_{MA,\mu_M}(\vec{r},R)$ follows from Eq. (2.6a). For $\rho \approx 0$ we have

$$\Phi^{(1)}_{as} = N_M(R) e^{-\gamma z} g^{-Z/\gamma} (2-g)^{-Z/\gamma}. \tag{3.3}$$

Equating the JWKB form, Eq. (3.1), and the asymptotic form (3.3) of the eigenfunction $\Phi^{(1)}_{MA,\mu_M}(\vec{r},R)$ in the central part of the S_F plane, where both these functions behave as $\exp(-\gamma z)$, we get

$$N_M(R) = \pi^{-1} \gamma^{1/2\gamma + 1/2} e^{1/4\gamma} 2^{-(2Z-1)/2\gamma + 1/4\gamma - 1} \times g^{n_{1M}} R^{1/4\gamma - 1/2} (2-g)^{Z/\gamma}. \tag{3.4}$$

Inserting expressions (3.4), (3.3), and (3.2) in Eq. (2.6a), we obtain the eigenfunction $\Phi^{(1)}_{MA,\mu_M}(\vec{r},R)$ on the whole moving Firsov plane, and for all asymptotic positions ($R \gg 1$) of this plane.

The obtained eigenfunction of the Hamiltonian $\hat{H}_1$ enables us to evaluate the time-dependent wave function $\Psi_1(\vec{r},t)$. Namely, inserting Eq. (2.6a) into Eq. (2.5) and taking into account that $\gamma = \gamma_{in} + O(1/R^2)$ and $n_{1M} = n_{1M,in}$, we get

$$\Psi_1(\vec{r},t) = N_M(R) \exp[-\gamma_{in} z - S_M(\vec{r},t) + i(\gamma^2_{in}/2)t], \tag{3.5a}$$

where $S_M(\vec{r},t) = s_M(\vec{r},R) - h_M(\vec{r},t) + i(\gamma^2_{in}/2)t$. The space-time correction factor $S_M(\vec{r},t)$ follows from the Schrödinger equation $i\partial\Psi_1/\partial t = \hat{H}_1 \Psi_1$, with the initial condition $\Psi_1(\vec{r},t) \to \Phi^{(1)}_{MA,\mu_{M,in}}(\vec{r},R)$ for $t \to t_{in} = 0$.

Using the approximations $\nabla^2 S_M \approx 0$ and $(\vec{\nabla} S_M)^2 \approx 0$, and performing the transformation $(z,t) \to (\xi_M, \eta_M)$, where $\xi_M = -(it + z/\gamma_{in})/2$ and $\eta_M = (-it + z/\gamma_{in})/2$, we get $-\partial S_M/\partial \xi_M = U_A + U_{AM}$. A particular solution of the last equation, satisfying the condition $S_M(\vec{r},t) \to 0$ for $t \to 0$, is given by the following expression:

$$S_M = \frac{Z}{iv + \gamma_{in}} \ln\left(\frac{\sqrt{\rho^2 + (R-z)^2} + R - z}{\sqrt{\rho^2 + R^2} + R} \right) - \frac{Z}{iv - \gamma_{in}} \ln\left(\frac{\sqrt{\rho^2 + (R+z)^2} + R + z}{\sqrt{\rho^2 + R^2} + R} \right). \tag{3.5b}$$

Equation (3.5a), with $S_M(\vec{r},t)$ and $N_M(R)$ given by Eqs. (3.5b) and (3.4), represents our final expression for the wave function $\Psi_1(\vec{r},t)$.

B. The function $\Psi_2(\vec{r},t)$ on the S_F plane

The function $\Psi'_2(\vec{r},t)$, Eq. (2.7a), evolves during the time t toward the large-l Rydberg state $\Phi^{(2)}_{A,\nu_{A,fin}}(\vec{r}_A)$, so that at intermediate stages of the ionic motion we have

$$\Psi'_2(\vec{r},t) = \exp[-S_A(\vec{r}_A,t) + i(\gamma^2_{A0}/2)t] \Phi^{(2)}_{A,\nu_{A,fin}}(\vec{r}_A), \tag{3.6}$$

where $S_A(\vec{r}_A,t) = s_A(\vec{r}_A,R) + i(\gamma^2_{A0}/2)t$; the factor $s_A(\vec{r}_A,R)$ originates from expression (2.8). We note that, for the large-l case, the Legendre polynomial in the hydrogenlike function $\Phi^{(2)}_{A,\nu_{A,fin}}(\vec{r}_A)$ can be expressed by the standard asymptotic form with respect to l.

The space-time correction factor $S_A(\vec{r}_A,t)$ can be obtained from the Schrödinger equation $i\partial\Psi'_2/\partial t = \hat{H}_2 \Psi'_2$, combined with the final condition $\Psi'_2(\vec{r},t) \to \Phi^{(2)}_{A,\nu_{A,fin}}(\vec{r}_A)$ when $t \to t_{fin} = \infty$. Using the approximations $\nabla^2 S_A \approx 0$ and $(\vec{\nabla} S_A)^2 \approx 0$, and performing the transformation $(r_A,t) \to (\xi_A, \eta_A)$, where $\xi_A = -(it + r_A/\gamma_{A0})/2$ and $\eta_A = (-it + r_A/\gamma_{A0})/2$, we get $-\partial S_A/\partial \xi_A = U_M + U_{AM}$.

The physically relevant particular solution for S_A can be obtained by the adiabatic limit requirement [10,11]: $S_A(\vec{r}_A,t) \to -[(2Z-1)/(4\gamma_{A0}R)] r_A + i(2Z-1)/(4v)$, for $v \to 0$. The solution satisfying the last condition is given by

$$S_A = \frac{\ln(z/R)}{4(iv - \gamma_{A0}\cos\Theta_A)} - \frac{Z}{\sqrt{C}} \ln\left(\frac{Z_1}{Z_0}\right) - \frac{2Z-1}{4\gamma_{A0}} + i\frac{2Z-1}{4v}, \tag{3.7}$$

where the angle Θ_A is defined in Fig. 1, whereas

$$C = \gamma^2_{A0} - 4v^2 - 4iv\gamma_{A0}\cos\Theta_A, \tag{3.8a}$$

$$Z_1 = 2\sqrt{C}\sqrt{\rho^2 + (z+R)^2} - 2r_A(\gamma_{A0} - 2iv\cos\Theta_A) + 4R(2iv - \gamma_{A0}\cos\Theta_A), \tag{3.8b}$$

$$Z_0 = 4R(\sqrt{C} + 2iv - \gamma_{A0}\cos\Theta_A). \tag{3.8c}$$

Equation (3.6), with the factor $S_A(\vec{r}_A,t)$ given by Eq. (3.7), represents our final expression for the time-dependent function $\Psi'_2(\vec{r},t)$.

C. The neutralization rate Γ^N and probability T^N

Physically relevant details of the electron-capture process at intermediate stages of the ion-surface interaction can be recognized by an explicit evaluation of the mixed flux $I(t)$, Eq. (2.3), as well as the neutralization rate $\Gamma^N(t)$ and probability $T^N(t)$, Eqs. (2.4a) and (2.4b). We shall focus on those space-time and energetic properties of the high-l process that are different from the low-l characteristics.

Using expressions (3.5a) and (3.6) for the states $\Psi_1(\vec{r},t)$ and $\Psi'_2(\vec{r},t)$, respectively, we get

$$I(t) = \frac{i}{2} \int_{S_F} \left[\gamma_{in} + \gamma_{A0} \frac{a}{r_A} + iv\left(1 - 2\frac{da}{dR}\right) \right] \times \Phi^{(2)*}_{A,\nu_{A,fin}} N_M e^{-\gamma_{in} z} e^{-S^*_A - S_M} e^{iwt} dS, \tag{3.9a}$$

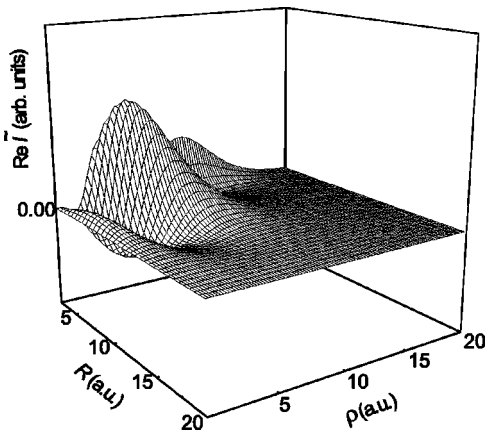

FIG. 2. $\mathrm{Re}\,\tilde{I}(R,\rho)$ as a function of ion-surface distance R and radial coordinate ρ for Cl VII ($v=2.50$ a.u.) ion with $n=7$ and $l=6$.

where $z=R-a$, whereas $w=(\gamma_{in}^2-\gamma_{A0}^2)/2-v^2(1-2a/R)/2$. Expression (3.9a), with the initial state $m_{M,in}=0$, is different from zero only for the Rydberg states with $m=0$, i.e., we have

$$I(t)=\int_0^\infty \tilde{I}(R,\rho)d\rho. \tag{3.9b}$$

Although expression (3.9b) is obtained under the asymptotic condition ($R\gg R_g=vt_g$), we can extend its validity over all ion-surface distances R with a sufficiently high accuracy. The errors due to extrapolation of the asymptotic forms of wave functions Ψ_1 and Ψ_2 to smaller values of R do not affect significantly the mixed flux $I(t)$, because of the variational method of determining the S_F-plane position [10].

In Fig. 2, we present the quantity $\mathrm{Re}\,\tilde{I}(R,\rho)$ as a function of R and ρ for the Cl VII ion with $n=7$, $l=6$, and the experimental value [13,14] of the ionic velocity ($v=2.50$ a.u.). The situation is similar for the $\mathrm{Im}\,\tilde{I}(t)$. From Fig. 2 we recognize that the electron transitions are mainly localized at the ion-surface distances $R\approx n$; note also that a wide region $\rho\approx R$ of the Firsov plane is active in the process.

The neutralization rate Γ^N of the Rydberg state $\nu_{A,fin}=(n,l,m=0)$ can be expressed in terms of the mixed flux $I(t)$ as follows:

$$\Gamma^{N,\mu_{M,in}}_{\nu_{A,fin}}(t)=\frac{2}{v}\left(\int_{R_g}^{R}\mathrm{Re}\,I(t)dR\right)\mathrm{Re}\,I(t) +\frac{2}{v}\left(\int_{R_g}^{R}\mathrm{Im}\,I(t)dR\right)\mathrm{Im}\,I(t). \tag{3.10}$$

The parameter R_g can be calculated by comparing the spectra of the Hamiltonians $\hat{H}_1(t)$ and $\hat{H}_2(t)$. Namely, we compare the position of the energy manifold of the Hamiltonian $\hat{H}_2(t)$, evolving into the final Rydberg level $E^{(2)}_{A,\nu_{A,fin}}=-Z^2/(2n^2)$ for $t=t_{fin}\to\infty$, with the conduction band of the solid. Taking into account that the common symmetry of the eigenproblems of both Hamiltonians is a parabolic one,

TABLE I. The numerical values of the coefficients $a_i=a_i(Z)$ for the ionic core charges $Z=6$, 7, and 8.

Z	6	7	8
a_0	9.77	2.84	0.27
a_1	1.80	0.56	0.10
a_2	4.13	1.12	0.12

we consider the parabolic splitting of the $\hat{H}_2(t)$ levels, i.e., at a given ion-surface distance $R\gg 1$, we have (see, for example, Ref. [7])

$$E^{(2)}_{A,\mu_A}(R)=-\frac{Z^2}{2n^2}+\frac{2Z-1}{4R}-\frac{3(Z-1)}{8Z}\,\frac{n(2n_{1A}-n+1)}{R^2}, \tag{3.11}$$

where $\mu_A=(n,n_{1A},m_A=0)$ and $n_{1A}=0,1,\ldots,n-1$.

For a given Z, the following three classes of the energy terms exist, depending on their behaviors with respect to the conduction band of the foil. The terms of the first class do not intersect the bottom ($-U_0$) of the conduction band, whereas the terms of the second class intersect the bottom and rapidly overflow the Fermi level. The third-class terms intersect the bottom, remaining below the Fermi level. We define the parameter R_g as the minimal value of the ion-surface distance at which the energy terms of the third class intersect the bottom of the conduction band:

$$R_g=\min[R|E^{(2)}_{A,\mu_A}(R)\pm\Delta E/2=-U_0], \tag{3.12}$$

where ΔE is the energy distance between the neighbor members of the manifold. The obtained values of R_g, for different n and for the experimentally relevant values of Z, are given by $R_g=a_0+a_1n+a_2n^2$, where the coefficients $a_i=a_i(Z)$ ($i=0,1,2$) are exposed in Table I.

In Fig. 3, we present the neutralization rate $\Gamma^{N,\mu_{M,in}}_{\nu_{A,fin}}=\Gamma^{\gamma}_{nl}$ per unit γ for the large-l Rydberg state $\nu_{A,fin}=(n,l,m=0)$ of the Cl VII ion as a function of the ion-surface distance R. For the γ values we take $\gamma=\gamma_m(n,l)$, which give the main contribution to the electron-capture

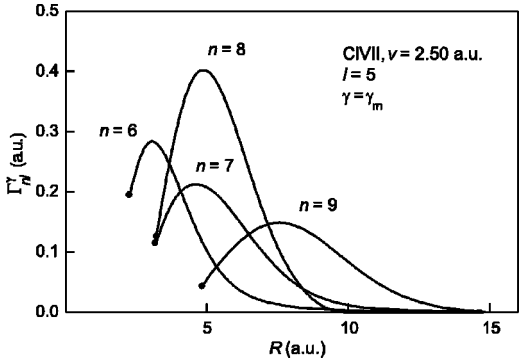

FIG. 3. The neutralization rates $\Gamma^{N,\mu_{M,in}}_{\nu_{A,fin}}=\Gamma^{\gamma}_{nl}$ (per unit γ) as a function of the ion-surface distance R for the Cl VII ($v=2.50$ a.u.) ion with $l=5$ and $\gamma=\gamma_m(n,l)$.

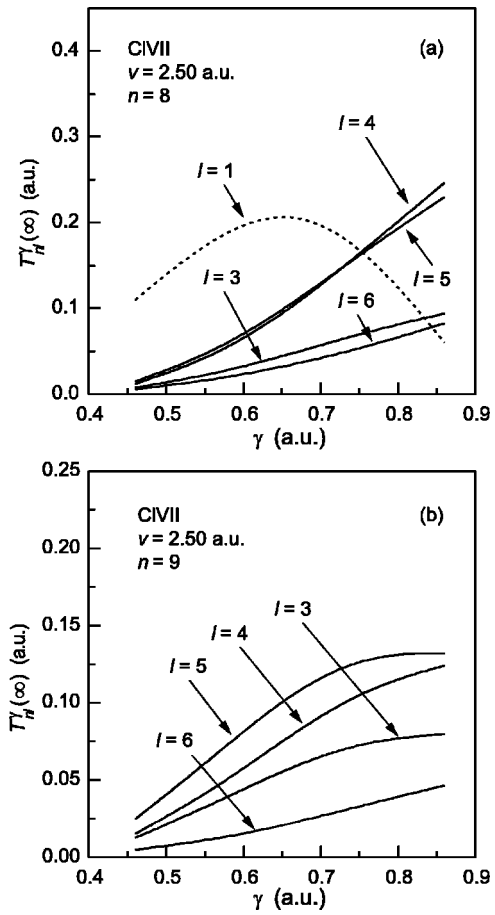

FIG. 4. Neutralization probabilities $T^{\gamma}_{nl}(\infty)$ (per unit γ) as a function of the energy parameter $\gamma \in (\gamma_F, \gamma_{U_0})$, for Cl VII ($v = 2.50$ a.u.) ion, for $n=8$ and $n=9$, respectively. The low-l result $l=1$ (dashed line) in Fig. 4(a) is taken from Ref. [11].

probability; see Fig. 4. From Fig. 3 we recognize the monotonic shift and lowering of position and height of the maximum, respectively, with the increase of the principal quantum number n for $6 \leqslant n \leqslant 9$. At the same time, the widths of the bell-shaped neutralization rates are increasing. The case $n=8$ is an exception. Consequently, the population of the large-l Rydberg states has a selective character, with maximum at $n \approx 8$.

The neutralization rates presented in Fig. 3 exhibit maxima at the critical distances $R_c \approx n$. We recall that the corresponding maxima [10,11] for the low-l Rydberg states are positioned at $R_c \approx 2n$. These results can be interpreted quasiclassically: the neutralization process takes place dominantly at those ion-surface distances where the quasiclassical orbital electronic motion (elliptic trajectory with the large half axis $n^2/Z \approx n$) is admissible.

For the intermediate ionic velocities $v \approx 1$ a.u. and the large angular momentums ($l=3,4,5, \ldots$), the electron-capture process is nonresonant in nature, i.e., all levels of the foil conduction band contribute to the final Rydberg state. In order to illustrate this fact, in Fig. 4 we present the neutralization probability $T^{\gamma}_{nl}(t) = \Sigma_{n_{1M}} T^{N,\mu_{M,in}}_{\nu_{A,fin}}(t)$ for $t \to \infty$ as a function of the energy parameter γ, in the range from $\gamma_F = \sqrt{2\phi}$, where ϕ is the foil work function, to $\gamma_{U_0} = \sqrt{2U_0}$. For the graphite foils, used in the experiments under consideration, we have [14,10,11] $\phi = 3$ eV and $U_0 = 10$ eV. As an example, we take again the Cl VII ion with $v = 2.50$ a.u.

From the curves presented we recognize a selective contribution of the conduction-band electrons. With the increase of the principal quantum number n, the maxima of the γ-distribution curves are shifted toward the Fermi level $\gamma = \gamma_F$; compare Figs. 4(a) and 4(b). The results concerning the γ contribution to the population of the large-l Rydberg states are different in comparison to the low-l results [11]. To point out this difference, in Fig. 4(a) we also represent the result for $l=1$ (dashed line). In Fig. 4, the monotonic rise of the neutralization probabilities with increasing l suddenly ceases at $l=6$. This is the position where the l distribution has a minimum.

The n selectivity of the electron-capture process on the R scale (Fig. 3) and the specific l behavior on the γ scale of Fig. 4 have a common origin in a complicate oscillatory character of the integrand $\tilde{I}(R,\rho)$ of Eq. (3.9b). More precisely, the electron-capture process dominates at critical ion-surface distance $R_c = R_c(n,l)$, whereas the ρ distribution of the mixed flux for $R = R_c$ is dominant for $\rho_c \approx n$, see Fig. 2. Accordingly, the function $\tilde{I}(R_c, \rho_c) = f(n,l)$ is an oscillatory function of n and l, and it generates the mentioned nonmonotonic features. This property of the mixed flux is a consequence of the two-state formalism, and could be interpreted as a "quantum interference" of the states $\Psi_1(\vec{r},t)$ and $\Psi_2(\vec{r},t)$. The interference pattern formed on the Firsov plane depends on quantum numbers n and l.

D. Comparison with experiments

The electron exchange during the intermediate stages of the ion-surface interaction results in the final Rydberg system (n,l) at $t_{fin} \to \infty$. The experimentally verifiable population probability P_{nl}, Eq. (2.4c), can be calculated explicitly for all relevant values of the ion-surface parameters.

The theoretical predictions will be compared with available experimental data [12–14] for the ions S VI, Cl VII, and Ar VIII. In the cited references, the relative level population probabilities have been measured and the curves reported were normalized by taking the fact that the $3p$ level population probability is a unity. The overall uncertainty of the experimental findings has been estimated [13] (around 20%). Mainly, two kinds of probability distribution graphs have been presented [12–14], depending on whether n or l is fixed. We shall focus on the l distributions.

Having in mind that the theory presented in this paper and our previous papers [10,11] is developed for the Rydberg states with $n \approx Z$ (accordingly, the $2p$ levels of the ionic projectiles are excluded), we choose a normalization that has been used previously [10,11] in our considerations of the low-l experimental curves. Accordingly, we normalize the experimental S VI data to the state $n=6$ and $l=1$, whereas the Cl VII curves are normalized to the state with $n=8$ and $l=1$; for the Ar VIII ions we take $n=10$ and $l=1$. The unified scaling of the experimental results adopted for both low-

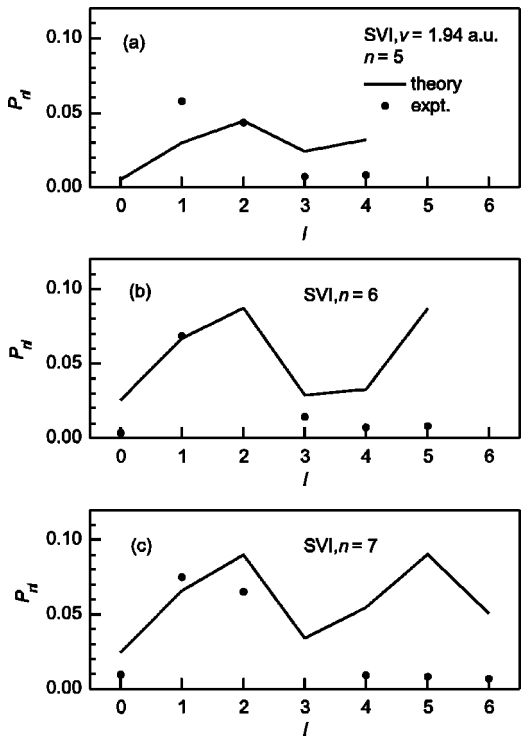

FIG. 5. Population probabilities P_{nl} of the Rydberg states (n,l) for the S VI ion ($v=1.94$ a.u.) with $n=5$, 6, and 7, respectively, as a function of the orbital quantum number $l \in [0, n-1]$. Dots are experimental data (Ref. [14]). The low-l results ($l=0,1,2$) are taken from Ref. [11].

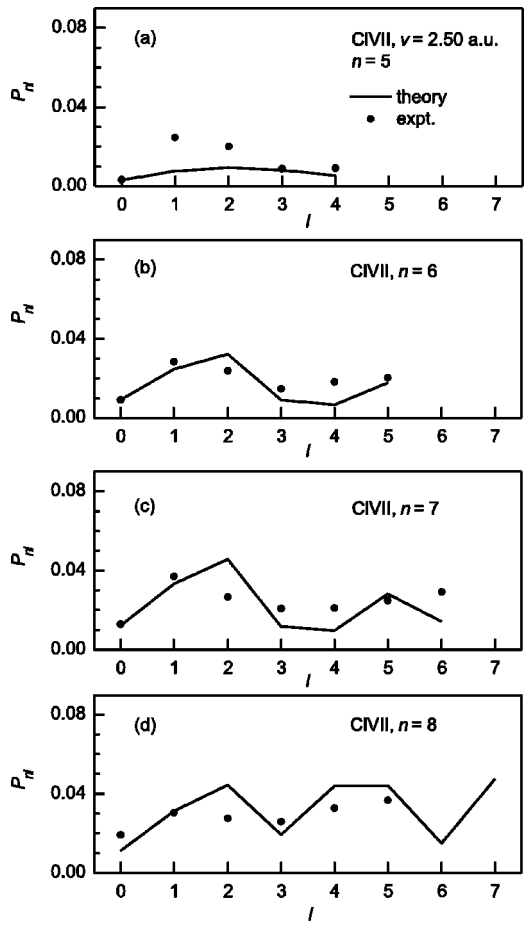

FIG. 6. Population probabilities P_{nl} of the Rydberg states (n,l) for the Cl VII ion ($v=2.50$ a.u.) with $n=5$, 6, 7, and 8, respectively, as a function of the orbital quantum number $l \in [0, n-1]$. Dots are experimental data (Refs. [13,14]). The low-l results ($l=0,1,2$) are taken from Ref. [11].

l and high-l values will enable us to establish a character of correlation between the theory and experiments for all values of l.

In Fig. 5, we present the l distributions of the probability P_{nl} for $n=5$, 6, and 7 of the S VI ion escaping the surface with the velocity $v=1.94$ a.u. In the same figure, we marked the experimental data [14] with dots. The theoretical probabilities in the low-l case ($l=0,1,2$), taken from Ref. [11], are also exposed in Fig. 5. The theoretical curves follow the experimental points almost over the whole l region, but an overestimation produced by our pure electron-capture model is evident around $l_{max}=n-1$ for $n=6$ in Fig. 5(b), as well as for $l=5$ and 6 in Fig. 5(c).

In Fig. 6, we expose the P_{nl} curves for the Cl VII ion with $n=5$, 6, 7, and 8. The experimental data [13,14] (dots) correspond to the ionic velocity $v=2.50$ a.u. The agreement between theory and experiments indicates that the electron-capture mechanism is sufficient for explaining the experimental facts presented in Figs. 6(a)–6(c). However, the experimental data from Fig. 6(d) report the l threshold at $l=l_{thr}=5$, suggesting that the reionization process [11,18] can completely destroy the states with $l=6$ and 7. Qualitatively, the l distributions presented in Fig. 6 can be compared with the l distributions [9] for $Z=7$, $n=6$, 7, and 8, obtained in the high velocity region ($v \approx 9$ a.u.), see Introduction. The l distributions of Ref. [9] (normalized to the $l=1$ data in Fig. 6) are significantly lower in the large-l region in comparison to our theoretical results.

Finally, in Fig. 7 we present the Ar VIII curves for $n=5$, 6, 7, and 8, with the velocity $v=1.42$ a.u. of the ionic projectile. The experimental data (dots) are taken from Ref. [12]. The low-l results [11] are presented together with the large-l cases discussed in the present paper. An overestimation for the case $l_{max}=7$ in Fig. 7(d) can be addressed to the reionization mechanism, as in the above-mentioned cases of S VI and Cl VII ions.

We also tested our electron-capture model for all other available experimental data concerning the higher-n Rydberg states of the ions S VI, Cl VII, and Ar VIII, not presented in Figs. 5–7. An agreement between theory and experiments has been found for all l distributions from $l=0$ to the experimentally established threshold values $l=l_{thr}<n-1$. However, beyond the l thresholds we found the same type of overestimation in our theoretical predictions as in the cases presented in Figs. 5(b,c), 6(d), and 7(c,d). This fact indicates that the nonresonant electron-capture mechanism, analyzed in this paper, is not sufficient for explaining the complexity of all experimental facts. What can be demonstrated within the framework of the two-state method is that the reionization [11] at intermediate stages of the ion-surface interaction

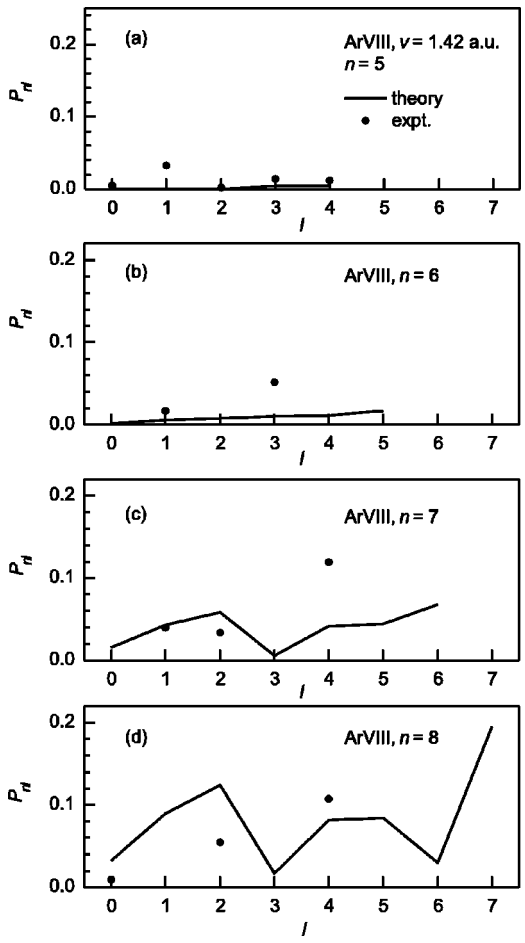

FIG. 7. Population probabilities P_{nl} of the Rydberg states (n,l) for the Ar VIII ion ($v=1.42$ a.u.) with $n=5$, 6, 7, and 8, respectively, as a function of the orbital quantum number $l \in [0, n-1]$. Dots are experimental data (Ref. [12]). The low-l results ($l=0,1,2$) are taken from Ref. [11].

is, generally, in a competition with the electron-capture mechanism (see Sec. IV).

The calculated population probabilities (Figs. 5–7) in most cases rise up to $l=2$ and then bend toward a minimum at $l=3$. Most of the experimental datasets, on the other hand, exhibit a maximum at $l=1$. This is due to the fact that in our graphical presentation the case $l=2$ has been considered as a low-l case, whereas the $l=3$ case is taken as the high-l result. Since the value $l=2$ is positioned in the matching region, more accurate theoretical P_{nl} values for $l=2$ could be obtained as a mean of the low-l and large-l results. These averaged values are in better correlation with the available experimental data.

IV. CONCLUDING REMARKS

The analysis presented in this paper represents an attempt of completion of our low-l results obtained previously [10,11] within the framework of the two-state model of the electron-capture process at solid surfaces. We consider the correlation of low-l and high-l results as a nontrivial fact, because technical details in our calculations concerning these l cases are based on rather different asymptotic methods. An experimentally obtained [12–14] deviation of the l distributions from the linear law $P_{nl} \sim 2l+1$ is supported by our model. The deviation becomes more pronounced in the high-l region for all tested ionic projectiles. Accordingly, under the experimental conditions discussed ($n \approx Z, v \approx 1$), the substates of the same Rydberg state are not [13] populated at random.

The extension of our model from low-l cases to large-l Rydberg states reflects the main physical differences between these two situations in the ion-surface system. Namely, in contrast to the low-l cases, a wide space region around the outgoing part of the ionic trajectory is active for the large-l Rydberg systems; this has been taken into account by the appropriate asymptotic procedure (Sec. II B). Also, the electron capture into the large-l states practically begins at $R_g = v t_g$, i.e., after a short period of very irregular variations of the mixed flux $I(t)$. Roughly speaking, the values obtained in Sec. III C are comparable with the mean distance between the foil atoms. Besides, in the nonresonant electron-capture process under the large-l conditions, the most active valence-band states of the solid are the states which are not close to the Fermi level.

Few additional concluding comments may be relevant for the Rydberg state population of multiply charged ionic projectiles under the beam-foil conditions discussed, as well as for some recent experimental results.

First, having faced the above-mentioned systematic trends in overestimation of the l distributions within the framework of the electron-capture model beyond the l thresholds, we performed an additional investigation [20] including the reionization mechanism [11,18] for large-l Rydberg states. A modified form of the ''renormalization'' procedure, used previously [11] for the explanation of n thresholds in experimentally observed population distributions, is developed. We found that the reionization will completely destroy those Rydberg states which are characterized by vanishing or very small eccentricities, resulting in the l thresholds observed in experiments. Moreover, the same reionization mechanism is also responsible for a lowering of the l distributions (around $l \approx l_{max} = n-1$) presented in Figs. 5(b,c), 6(d), and 7(c,d).

Second, we found that the cited references [12–14] give a sufficiently complete amount of relevant information for a comparison with the theoretical results of the present paper. A most direct extrapolation of the presented results to other beam-foil experiments at intermediate velocities is related to the large-l distributions of Xe VIII, reported in Ref. [21]. Also, the obtained large-l results can be applied in investigations of the velocity dependence on the population probability $P_{nl} = P_{nl}(v)$ around $v \approx 1$ and compared with the beam-foil experimental results given in Ref. [22].

Third, one of recent ion-surface experiments (see, for example, Refs. [23,24]) was performed in the scattering geometry and a total yield of the scattered multiply charged ions has been measured. Accordingly, specific quantum features concerning the l distributions of the Rydberg states, discussed in our model, cannot be tested directly by these experiments. On the other hand, in the beam-foil experiment

[25] only the population dynamics of internal states of the multiply charged ions has been reported, so that the ion-surface effects discussed in the present paper could give only the second-order contributions to the measured quantities.

Finally, an additional direction of experimental investigations (see, for example, Ref. [26]) is devoted to the Rydberg atoms. These experiments were performed with hyperthermal beams in the nearly grazing geometry. The two-state model adapted to this experimental situation could be applied in the adiabatic limit $v \ll 1$.

ACKNOWLEDGMENTS

This work was supported in part by the Ministry of Development, Science and Technologies, Republic of Serbia (Project No. 1470).

[1] J. Burgdörfer, in *Review of Fundamental Processes and Applications of Atoms and Molecules*, edited by C.D. Lin (World Scientific, Singapore, 1997).
[2] J. Burgdörfer, P. Lerner, and F. Meyer, Phys. Rev. A **44**, 5674 (1991).
[3] J. Ducrée, F. Casali, and U. Thumm, Phys. Rev. A **57**, 338 (1998).
[4] J. Ducrée, H.J. Andrä, and U. Thumm, Phys. Rev. A **60**, 3029 (1999).
[5] U. Wille, Phys. Rev. B **50**, 1888 (1994).
[6] P. Kürpick and U. Thumm, Phys. Rev. A **54**, 1487 (1996).
[7] A. Borisov, R. Zimny, D. Teillet-Billy, and J. Gauyacq, Phys. Rev. A **53**, 2457 (1996).
[8] P. Nordlander, Phys. Rev. B **53**, 4125 (1996).
[9] J. Kemmler, J. Burgdörfer, and C.O. Reinhold, Phys. Rev. A **44**, 2993 (1991).
[10] N.N. Nedeljković, Lj.D. Nedeljković, S.B. Vojvodić, and M.A. Mirković, Phys. Rev. B **49**, 5621 (1994).
[11] Lj.D. Nedeljković and N.N. Nedeljković, Phys. Rev. B **58**, 16 455 (1998).
[12] S. Bashkin, H. Oona, and E. Veje, Phys. Rev. A **25**, 417 (1982).
[13] E. Veje, Nucl. Instrum. Methods Phys. Res. B **9**, 586 (1985).
[14] E. Veje and H. Winter, Z. Phys. D: At., Mol. Clusters **10**, 457 (1988).
[15] N.N. Nedeljković, Lj.D. Nedeljković, R.K. Janev, and Z.L. Mišković, Nucl. Instrum. Methods Phys. Res. B **58**, 519 (1991).
[16] Yu.N. Demkov and V.N. Ostrovskii, Zh. Eksp. Teor. Fiz. **69**, 1582 (1975).
[17] J. Bardeen, Phys. Rev. Lett. **6**, 57 (1961).
[18] Lj.D. Nedeljković and N.N. Nedeljković, Phys. Rev. A **67**, 032709 (2003).
[19] N.N. Nedeljković, Fizika (Zagreb) **12**, 275 (1980).
[20] N.N. Nedeljković, Lj.D. Nedeljković, and M.A. Mirković (unpublished).
[21] R. Hallin, J.A. Leavitt, A. Lindgard, P.W. Rathmann, H. Vach, and E. Veje, Nucl. Instrum. Methods Phys. Res. **41**, 202 (1982).
[22] C. Jupen, B. Denne, J.O. Ekberg, L. Engstrom, U. Litzen, I. Martinson, W. Tai-Meng, A. Trigueiros, and E. Veje, Phys. Rev. A **26**, 2468 (1982).
[23] S. Kyoh, K. Takakuwa, M. Sakura, M. Umezawa, A. Itoh, and N. Imanishi, Phys. Rev. A **51**, 554 (1995).
[24] Q. Yan, D. Zehner, F.W. Meyer, and S. Schippers, Phys. Rev. A **54**, 641 (1996).
[25] T. Minami, C.O. Reinhold, M. Seliger, J. Burgdörfer, C. Fourment, E. Lamour, J. Rozet, D. Vernhet, and B. Gervais, Phys. Rev. A **65**, 032901 (2002).
[26] S.B. Hill, C.B. Haich, Z. Zhou, P. Nordlander, and F.B. Dunning, Phys. Rev. Lett. **85**, 5444 (2000).